Topological charge analysis of ultrafast single skyrmion creation

Gen Yin,[1] Yufan Li,[2] Lingyao Kong,[3] Roger K. Lake,[1,*] C. L. Chien,[2] and Jiadong Zang[4,*]
[1]*Department of Electrical and Computer Engineering, University of California, Riverside, California 92521-0204, USA*
[2]*Department of Physics and Astronomy, Johns Hopkins University, Baltimore, Maryland 21218, USA*
[3]*State Key Laboratory of Surface Physics and Department of Physics, Fudan University, Shanghai 200443, China*
[4]*Department of Physics, University of New Hampshire, Durham, New Hampshire 03824, USA*
(Received 20 October 2014; revised manuscript received 13 April 2016; published 2 May 2016)

Magnetic skyrmions are topologically nontrivial spin textures of potential interest for future information storage applications, and for such purposes, the control and understanding of single skyrmion creation is required. A scheme is analyzed to create single Néel-type and Bloch-type skyrmions in helimagnetic thin films utilizing the dynamical excitations induced by the Oersted field and the spin transfer torque given by a vertically injected spin-polarized current. A topological charge analysis using a lattice version of the topological charge provides insight into the locally triggered transition from a trivial to a nontrivial topological spin texture of the Néel or Bloch type skyrmion. The topological protection of the magnetic skyrmion is determined by the symmetric Heisenberg exchange energy. The critical switching current density is $\sim 10^7$ A/cm^2, which decreases with the easy-plane type uniaxial anisotropy and thermal fluctuations. The in-plane spin polarization of the injected current performs better than out-of-plane polarization, and it provides ultrafast switching times (within 100 ps) and reliable switching outcomes.

DOI: 10.1103/PhysRevB.93.174403

I. INTRODUCTION

Magnetic skyrmions are topologically protected spin textures in which the local moments on a two-dimensional lattice points in all directions with a topologically nontrivial mapping to the unit sphere [1,2]. Physically, each skyrmion is a circular spin texture in which the spins on the periphery are polarized vertically, the central spin is polarized in the opposite direction, and, in between, the spins smoothly transition between the two opposite polarizations. A swirling transition, which is effectively a circle of double Bloch-type domain walls, gives a Bloch-type skyrmion. This type of skyrmion was first discovered in the temperature-magnetic field (T-H) phase diagram of B20 magnets [3–5]. In these materials, the atomic structure of the lattice breaks the inversion symmetry, inducing an asymmetric Dzyaloshinsky-Moriya (DM) exchange interaction [6,7]. The competition between the DM exchange and the symmetric Heisenberg exchange stablizes the skyrmion phase in these materials. A Néel-type skyrmion, on the other hand, is a wrapped double Néel-wall. Such a skyrmion is stabilized by an interfacial DM interaction, which is originated from the broken interfacial inversion symmetry. This type of DM interaction is usually observed at the interface between a magnetic thin film and a layer of heavy metal with strong spin-orbit coupling (SOC). For both types of skyrmions, the radius, ranging from about 3 to 100 nm [3–5,8], is determined by the ratio of the strengths of the DM interaction and the Heisenberg interaction [9].

Skyrmion lattices and isolated skyrmions in both bulk and thin films have been observed by neutron scattering [3,10], Lorentz transmission electron microscopy [4,5,11–13], and spin-resolved scanning tunneling microscopy (STM) [14]. Current can drive skyrmion spin textures with a current density 4-5 orders of magnitude lower than that required to move conventional magnetic domain walls [12,15–17]. This suggests promising spintronic applications exploiting the topological spin texture as the state variable [18–20].

A two-dimensional skyrmion lattice may be formed under a uniform magnetic field [3,4], however, the switching of isolated, individual skyrmions is far more challenging. The single skyrmion switching was first experimentally demonstrated by injecting spin-polarized current from an STM tip into ultrathin Pd/Fe/Ir(111) films at 4.2 K [21]. Other schemes of single skyrmion switchings, such as using a sharp notch [20], a circulating current [22], thermal excitations [23] and spin-orbit torques (SOTs) [19] have been proposed. Spintronic applications call for on-wafer solutions to precisely control the position and the time of skyrmion switchings with good reliability. This is rather difficult because each switching event corresponds to a topological transition, which has to break the protection given by the topological order. This process has to overcome the topological protection barrier, which is both energetically unfavorable and difficult to manipulate.

In this paper, we theoretically investigate the topological transition of the microscopic spin texture during a dynamical skyrmion creation process. This picture provides insight into the critical condition to create isolated skyrmions and a quantitative understanding in the topological barrier. Based on this picture, we propose that controlled skyrmion creation can be realized by the spin transfer torques (STTs) induced from a magnetic electrode. Such a geometry and creation mechanism is applicable to both the Bloch-type and the Néel-type skyrmions, and is potentially compatible with the standard metal process used in silicon integrated circuits.

II. TOPOLOGICAL TRANSITION ANALYSIS

The critical condition of the topological transition is determined by the topological charge evolution during a

*Authors to whom correspondence should be addressed: rlake@ee.ucr.edu, jiadong.zang@unh.edu

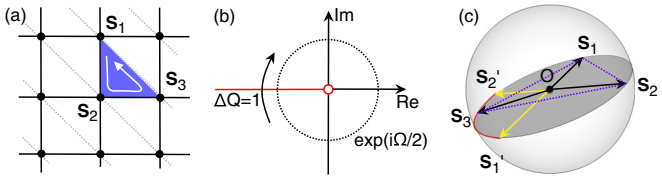

FIG. 1. The critical conditioon of a topological transition. (a) Triangulated square lattice. $\mathbf{S}_1$, $\mathbf{S}_2$ and $\mathbf{S}_3$ follow a counter-clockwise order on each triangle grid. (b) $\exp(\frac{i\Omega}{2})$ on the complex plane. The branch cut is denoted by the red line on the negative real axis. (c) A typical spin configuration at the moment of a topological transition. It only occurs when $\mathbf{S}_3$ crosses the geodesic $\mathbf{S}_1'\mathbf{S}_2'$ (red arc). $\mathbf{S}_1'$ and $\mathbf{S}_2'$ are the point reflection images of $\mathbf{S}_1$ and $\mathbf{S}_2$ about the sphere center.

spin dynamical process. A skyrmion is distinguished from a ferromagnet or other trivial state by the topological charge Q, which is a nonvanishing integer describing the winding number of the 2+1 dimensional classical spin [$\Pi_2(S^2)$ homotopy group], in analogy to the 3+1 dimensional topological soliton [$\Pi_3(S^3)$] originally introduced by Skyrme *et al.* [24–26]. Each skyrmion contributes ± 1 to the total topological charge. Usually $Q = \frac{1}{4\pi}\int d^2r\mathbf{S}\cdot(\partial_x\mathbf{S}\times\partial_y\mathbf{S})$ is employed, but it is well defined only in the continuum limit where all the spins are almost parallel to their neighbors [25]. In this limit, magnetic dynamical processes can only distort the geometry of the spin texture, but cannot change the wrapping number in the spin space. Thus, the topological charge above is conserved, and can not capture the precise time evolution of the topological transition.

Here, we employ the lattice version of the topological charge that provides a microscopic picture of the spin evolution and reveals the microscopic criteria for a topological transition to occur during any dynamical process. This version of Q was first introduced by Berg *et al.* [27], which is defined on a square lattice mesh illustrated in Fig. 1(a). The calculation of Q starts by triangulating the entire lattice and then counting the solid angles $\Omega_\triangle$ for each triangle $\triangle(\mathbf{S}_1,\mathbf{S}_2,\mathbf{S}_3)$ determined by

$$\exp\left(i\frac{\Omega_\triangle}{2}\right) = \rho^{-1}[1+\mathbf{S}_1\cdot\mathbf{S}_2+\mathbf{S}_2\cdot\mathbf{S}_3+\mathbf{S}_3\cdot\mathbf{S}_1 + i\mathbf{S}_1\cdot(\mathbf{S}_2\times\mathbf{S}_3)], \quad (1)$$

where $-2\pi<\Omega<2\pi$ and $\rho=[2(1+\mathbf{S}_1\cdot\mathbf{S}_2)(1+\mathbf{S}_2\cdot\mathbf{S}_3)(1+\mathbf{S}_3\cdot\mathbf{S}_1)]^{1/2}$ is the normalization factor [27]. The lattice version of the topological charge Q is then given by summing over all of the triangles:

$$Q=\frac{1}{4\pi}\sum_\triangle\Omega_\triangle. \quad (2)$$

From this definition, the directional solid angle $\Omega_\triangle$ ranges from -2π to 2π so that the negative real axis of the complex plane in Eq. (1) is a branch cut. The exponential $e^{i\Omega_\triangle/2}$ lies on the branch cut in the complex plane when $\mathbf{S}_1\cdot(\mathbf{S}_2\times\mathbf{S}_3)=0$, and $1+\mathbf{S}_1\cdot\mathbf{S}_2+\mathbf{S}_2\cdot\mathbf{S}_3+\mathbf{S}_3\cdot\mathbf{S}_1<0$. $\Omega_\triangle$ is 2π immediately above, and -2π immediately below, the branch cut. Any dynamical process causing $e^{i\Omega_\triangle/2}$ to cross the branch cut is accompanied by a change in the topological charge of ±1 as shown in Fig. 1(b). To trigger an event crossing the branch cut, the dynamical process must drive three spins $\mathbf{S}_1$, $\mathbf{S}_2$, $\mathbf{S}_3$ in one particular triangle coplanar from the condition $\mathbf{S}_1\cdot(\mathbf{S}_2\times\mathbf{S}_3)=0$. The other condition $1+\mathbf{S}_1\cdot\mathbf{S}_2+\mathbf{S}_2\cdot\mathbf{S}_3+\mathbf{S}_3\cdot\mathbf{S}_1<0$ leads to the inequality $(\mathbf{S}_1-\mathbf{S}_2)\cdot(\mathbf{S}_3-\mathbf{S}_2)>0$, so that $\angle\mathbf{S}_1\mathbf{S}_2\mathbf{S}_3$ is an acute angle, and the same holds true for permutations of the three indices 1, 2, and 3. Consequently, three spins must point 'away' from each other at the branch cut. For fixed $\mathbf{S}_1$ and $\mathbf{S}_2$, $\mathbf{S}_3$ must lie on the arc $\mathbf{S}_{1'}\mathbf{S}_{2'}$ as shown in Fig. 1(c). This coplanar but highly noncollinear critical state must be achieved during skyrmion switching events.

Based on this switching criteria, the energy barrier protecting the topological charge is identified, and can thus be quantified. The full spin Hamiltonian of a magnetic helix is given by

$$H=\sum_{\langle i,j\rangle}\left[-J\mathbf{S}_i\cdot\mathbf{S}_j+H_{i,j}^{\mathrm{DM}}\right]-\mu_0\sum\mathbf{S}_i\cdot\mathbf{H}_{\mathrm{Ost}}, \quad (3)$$

where

$$\begin{cases} H_{i,j}^{\mathrm{DM}}=D\hat{\mathbf{r}}_{ij}\cdot(\mathbf{S}\times\mathbf{S}_j) & \text{(Bloch type)}\\ H_{i,j}^{\mathrm{DM}}=D(\hat{\mathbf{z}}\times\hat{\mathbf{r}}_{ij})\cdot(\mathbf{S}_i\times\mathbf{S}_j) & \text{(Néel type)}\end{cases}.$$

The two terms in the square bracket are the Heisenberg and DM interactions, respectively, and the last term is the Zeeman coupling. $\hat{r}_{ij}$ denotes the unit vector pointing from $\mathbf{S}_i$ to $\mathbf{S}_j$. At the moment of switching, three spins on one particular triangle are coplanar, and the DM interaction does not contribute to the total energy. The energy of this particular triangle, measured from the ferromagnetic state, is thus given by

$$\Delta\epsilon=J\left(1-\frac{\mathbf{S}_1\cdot\mathbf{S}_2}{2}-\frac{\mathbf{S}_2\cdot\mathbf{S}_3}{2}\right)+\mathbf{B}_{\mathrm{Ost}}\cdot\left(\frac{1}{2}-\frac{\mathbf{S}_1+\mathbf{S}_2+\mathbf{S}_3}{6}\right). \quad (4)$$

Since the spins at the transition are highly noncollinear, the exchange becomes very large, and the Zeeman coupling in the second term in Eq. (4) is thus negligible. From the topological transition requirement, $1+\mathbf{S}_1\cdot\mathbf{S}_2+\mathbf{S}_2\cdot\mathbf{S}_3+\mathbf{S}_3\cdot\mathbf{S}_1<0$, it can be obtained that $-J(\mathbf{S}_1\cdot\mathbf{S}_2+\mathbf{S}_2\cdot\mathbf{S}_3)>J(1+\mathbf{S}_3\cdot\mathbf{S}_1)\geqslant 0$. Thus $\Delta\epsilon>J$ has to be satisfied. The maximum value of $\Delta\epsilon=2J$ occurs when $\mathbf{S}_2$ is antialigned with both $\mathbf{S}_1$ and $\mathbf{S}_3$, such that $J<\Delta\epsilon<2J$. In different switching processes, the actual value of this barrier varies within this range, determined by the exact spin configurations at the moment of the transition. Since this criteria comes from the generic topological charge analysis, it applies for both the Bloch-type and the Néel-type skyrmions.

III. SINGLE SKYRMION CREATION DUE TO A VERTICAL CURRENT

Our proposed scheme to control the precise location and the moment of the topological transition is illustrated in Fig. 2. A metallic, nonmagnetic (usually copper) nanopillar electrode of radius R is deposited on top of a helimagnetic thin film, with a back contact on the bottom of the film which serves as the drain of the electron current. In order to polarize the injected current, a magnetic layer is deposited on top of the copper spacer. The angle between the polarization and the x-y plane is θ. A uniform external magnetic field $\mathbf{H}_0$ is always applied vertically to ensure a ferromagnetic ground state in which all

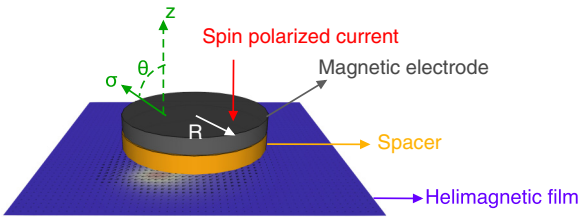

FIG. 2. The sandwich structure of the proposed skyrmion creation scheme. θ is the angle between the injected spin $\boldsymbol{\sigma}$ and the z axis.

spins are perpendicularly polarized. In order to quantitatively evaluate the required condition and the feasibility, dynamical simulations of the spin system based on the Landau-Lifshitz-Gilbert (LLG) equation are performed. The equation of motion is given by

$$\dot{\mathbf{S}} = -\gamma \mathbf{S} \times \mathbf{H}_{\text{eff}} + \alpha \mathbf{S} \times \dot{\mathbf{S}} + \boldsymbol{\tau}_{\text{STT}}, \tag{5}$$

where $\gamma = g/\hbar$ is the gyromagnetic ratio and α is the Gilbert damping coefficient. $\mathbf{H}_{\text{eff}}$ is the effective field given by $\mathbf{H}_{\text{eff}} = -\partial H/\partial \mathbf{S}$. A fourth order Runge-Kutta algorithm is employed to integrate this first order differential equation. In our simulation, material parameters of FeGe are applied, such that $J = aA_0$ and $D = a^2 D_0$, where $a = 2.3$ nm is the choice of the mesh grid size, $A_0 = 5.33$ meV Å^{-1} is the exchange stiffness and $D_0 = 0.305$ meV Å^{-2} is the DM interaction density. These parameters are chosen such that the simulated helical state period matches with the experimental observation $\lambda = 2\pi a/\arctan(D/\sqrt{2}J) = 70$ nm. The STT term is written as $\tau_{\text{STT}} = -j\frac{\gamma\hbar p}{2e\mu_0 M_s t}[\mathbf{S} \times (\mathbf{S} \times \boldsymbol{\sigma})]$ [28], where p is the polarization, j is the current density, $\boldsymbol{\sigma}$ is the injected spin orientation, $M_s = 10^5$ A m^{-1} is the saturation magnetization and t is the film thickness. A background field $\mathbf{H}_0$ is applied along the $\hat{z}$ direction, perpendicular to the thin film, such that the energy of a FM state matches the energy of a single skyrmion.

A. Oersted field induced creation

First, we consider the creation of a Bloch-type skyrmion by the injection of spin *unpolarized* current, where all the excitations in the spin texture are induced by the Oersted field associated with the vertical current. Starting from a ferromagnetic (FM) initial state, an unpolarized DC current is injected at $t = 0$. This generates a swirling Oersted field in the plane of the helimagnetic thin film, dragging the spins into a swirling spin texture, which eventually evolve to a single skyrmion at the center. The spin textures before and after this topological transition are shown in Figs. 3(a) and 3(b). At the center of the swirling texture, the central spin, $\mathbf{S}_0$, and its four nearest neighbors $\mathbf{S}_A$, $\mathbf{S}_B$, $\mathbf{S}_C$, and $\mathbf{S}_D$ form a configuration illustrated in Fig. 3(c). Due to the rotational symmetry of the applied field, these four spins relate to each other by successive rotations of $\pi/2$ about the $\hat{z}$ axis. They thus share the same angle θ to the plane of the film, and the same azimuthal angle φ measured from the x or y axis, respectively. In the case of a Bloch-type skyrmion, the effective field experienced by the central spin is along the z direction with an amplitude of $H^0_{\text{eff}} = 4J \sin\theta - 4D \cos\theta \sin\varphi + H_0$,

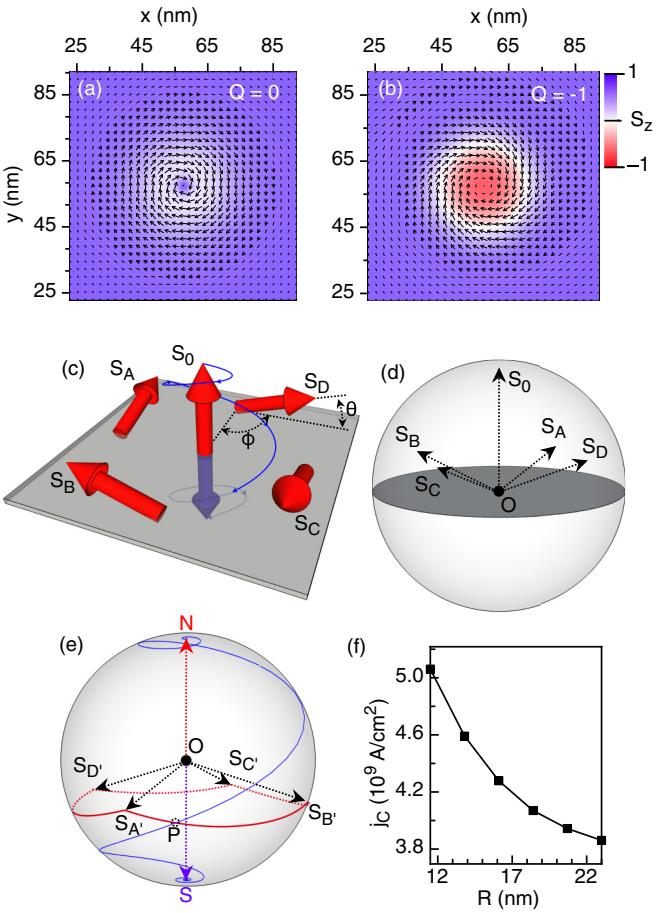

FIG. 3. Single Bloch-type skyrmion creation due to an Oersted field induced by spin unpolarized current. (a) The swirling texture before the creation of a skyrmion. (b) The spin texture after a topological charge of -1 is created. (c) The real-space spin configuration at the center of the swirling texture, immediately before the creation moment. (d) The spin configuration in spin space. (e) The trajectory of $\mathbf{S}_0$ during the creation process. The closed loop $\mathbf{S}_{A'}\mathbf{S}_{B'}\mathbf{S}_{C'}\mathbf{S}_{D'}$ illustrates the boundary of the topological transition. (f) The critical current density j_C at different values of the electrode radius.

where J and D are the strength of the Heisenberg and the DM interaction, respectively. The direction of the electrical current is chosen so that the swirling direction of the circulating field is the same as that of the in-plane spin component of a skyrmion; therefore φ is about $\pi/2$, and $\sin\varphi$ is positive. Before a skyrmion can be created, the circulating field pulls spins $\mathbf{S}_A$, $\mathbf{S}_B$, $\mathbf{S}_C$, and $\mathbf{S}_D$ downward towards the plane reducing the angle θ. H^0_{eff} therefore decreases accordingly, but still remains positive. When θ reaches a critical threshold as the four spins rotate towards the plane, H^0_{eff} reverses its sign, and as a result, spin $\mathbf{S}_0$ quickly flips down into the $-z$ direction. This process changes the topological charge by an integer and thus creates a skyrmion. Note that the contribution from the DM interaction in Néel-type skyrmions cannot generate a negative term in H^0_{eff}, therefore the swirling Oersted field can only create a Bloch-type skyrmion.

To demonstrate this process, we draw $\mathbf{S}_0$ and its nearest neighbors, $\mathbf{S}_A$, $\mathbf{S}_B$, $\mathbf{S}_C$, and $\mathbf{S}_D$, in a unit sphere at the

critical state immediately before the reversal of the central spin [Fig. 3(d)]. $\mathbf{S}_{A'}$, $\mathbf{S}_{B'}$, $\mathbf{S}_{C'}$ and $\mathbf{S}_{D'}$ are the mirror points of $\mathbf{S}_A$, $\mathbf{S}_B$, $\mathbf{S}_C$, and $\mathbf{S}_D$ with respect to the sphere center [Fig. 3(e)]. Both planes $\mathbf{S}_A\mathbf{S}_B\mathbf{S}_C\mathbf{S}_D$ and $\mathbf{S}_{A'}\mathbf{S}_{B'}\mathbf{S}_{C'}\mathbf{S}_{D'}$ are parallel with the equatorial plane, and the four points in each plane are equidistant. Through a fast process, $\mathbf{S}_0$ rapidly switches from the north pole (N) to the south pole (S). When $\mathbf{S}_0$ is located on the geodesic arc $\mathbf{S}_{A'}\mathbf{S}_{B'}$ shown as point P in Fig. 3(e), the three spins $\mathbf{S}_A$, $\mathbf{S}_B$, and $\mathbf{S}_0$ are coplanar. As $\mathbf{S}_0$ crosses arc $\mathbf{S}_{A'}\mathbf{S}_{B'}$, the solid angle formed by the three spins changes sign resulting in a change in $\Omega_\triangle$ of 4π and a change in the topological charge in Eq. (3) of 1. The same process applies to the other arcs $\mathbf{S}_{B'}\mathbf{S}_{C'}$, $\mathbf{S}_{C'}\mathbf{S}_{D'}$, and $\mathbf{S}_{D'}\mathbf{S}_{A'}$. Notice that these four arcs form a closed loop enclosing the south pole as shown by the red curve in Fig. 3(c). Therefore, the trajectory of $\mathbf{S}_0$ must cross this closed loop once, and an integer change of the topological charge is guaranteed regardless of the actual geometry of the $\mathbf{S}_0$ trajectory. A single skyrmion is thus created.

The critical current density, j_C, to trigger the topological charge is shown in Fig. 3(f). The value of j_C is on the order of 10^9 A/cm^2, which is three orders of magnitudes larger than the typical switching current density applicable to integrited circuits. An increase in the electrode radius of several nanometers can reduce j_C, but it cannot provide improvements by orders of magnitudes.

B. Spin transfer torque (SST) driven switching

Since the threshold current is so high, skyrmion creation due to a pure Oersted field is not practical. Spin-polarization of the injected current can reduce the threshold current density by one order of magnitude. In this case, the dynamical process is dominated by the STT, which has been proposed to be a promising mechanism to switch nano-magnets in spintronic integrited circuits [29].

Several snap shots of this dynamical process are shown in Fig. 4. After the current is turned on, the STT and the Oersted field drive the spins into the x-y plane near the electrode. Since spins at the periphery deviate from the outside FM configuration, the DM energy starts to increase. This drives the spin texture to form a bubble-like domain, in which the center spins present negative z components, while the spins at the periphery give large in-plane components. The bubblelike domain then continues to grow and starts to wrap into a circular domain wall with a singularity. Around the singularity, the spins gradually develop into an antiparallel configuration, which then generate a quick, drastic dynamical process that creates a topological charge of -1. In contrast to the creation induced by pure Oersted fields, the STT triggerred creation works with both Bloch and Néel type skyrmions. Movies containing the details of this dynamical process are available in Ref. [30]. The spin trajectories corresponding to the local topological transition are shown in Fig. 4(e), which follows the coplanar and noncollinear configuration discussed in the previous section.

The critical current density to trigger the skyrmion creation event is evaluated through a series of LLG simulations. For a low current density, excitations damp away very fast, and no skyrmion is created. The creation of skyrmions occurs only when the current density reaches a critical value j_C. The phase

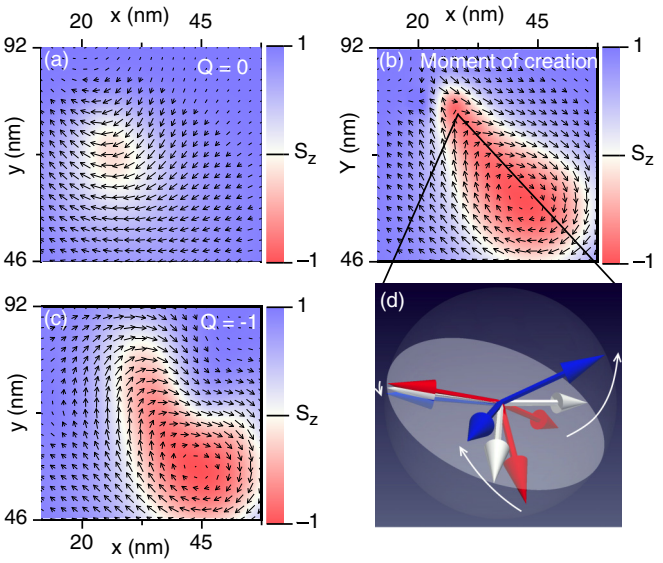

FIG. 4. (a)–(c) are snap shots of the spin texture several picoseconds around the moment of the topological transition in a Bloch-type helimagnet thin film. (d) demonstrates the spin trajectories of the local topological transition. The red and blue arrows denote the configurations before and after the transition, respectively. A coplanar and noncolinear configuration is achieved exactly at the moment of the skyrmion creation (white arrows).

diagram of j_C is a function of the spin polarization angle θ and the electrode radius R, as shown in Fig. 5. Here R varies from 11.5 to 25.3 nm, while the polarization of the injected current is modifed from $-\hat{z}$ to the x-y plane ($90^\circ < \theta < 180^\circ$). The skyrmion creation does not happen when $\theta < 90^\circ$. In this

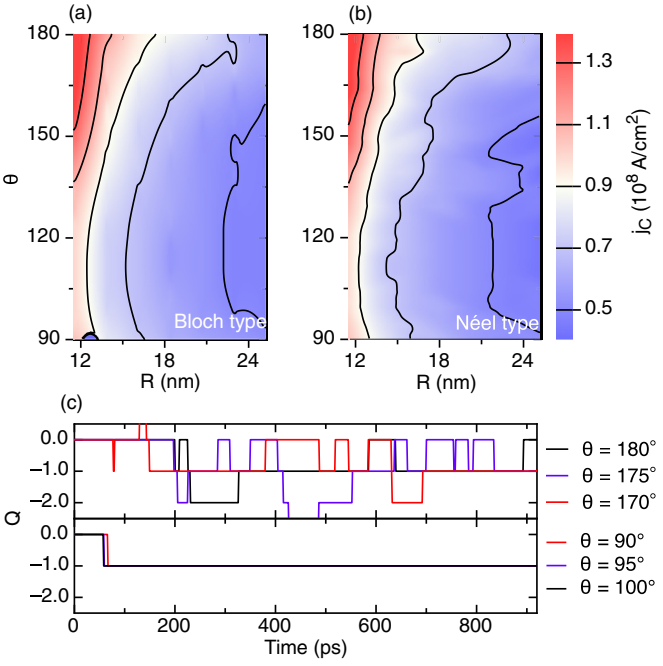

FIG. 5. The phase diagram of j_C for the (a) Bloch-type and the (b) Néel-type skyrmions. (c) The time evolution of the topological charge at several different polarization angles in the case of Bloch-type skyrmions.

calculation, both the Néel-type and the Bloch-type skyrmion creations are examined using the same set of parameters. Despite the differences in the spin dynamical details, the phase diagrams for the two types of skyrmions are quite similar. The minimum current density occurs at $\theta \sim 110^\circ$, where the polarization is close to the in-plane case. For both skyrmion types, j_C is approximately 10^8 A/cm^2, which is similar to the critical switching current density due to spin orbit torques estimated by previous numerical estimates. Increasing the electrode radius can further decrease the current density but only on a linear scale rather than an exponential scale.

The reliability and the dynamical details of the switching process significantly depends on θ, the orientation of the spin polarization. The STT can generate an "antidamping" effect during the precession of the local magnetic moment when the injected spin is antiparallel to the precession axis [31]. The antidamping can either induce a consistent oscillation or even the switching of a single-domain nanomagnet. This is similar to the switching of a single skyrmion in our proposed scheme. In the case of $\theta < 90^\circ$, the excitations induced by the torque damp away so quickly that no topological transition could occur with a reasonable current density. In the case of $90^\circ < \theta < 180^\circ$, switching becomes possible. Since the STT is given by $\mathbf{S} \times (\mathbf{S} \times \boldsymbol{\sigma})$, the maximum value of the torque at $t = 0$ occurs when $\theta = 90^\circ$. The torque becomes zero in the case of $\theta \to 180^\circ$, where the required current density reaches its maximum in the phase diagram. In the case of a large θ, the dynamical effect continues after the skyrmion is created, where the oscillation of the topological charge occurs. The time evolution of the topological charge of a Bloch-type skyrmion is presented in Fig. 6(b), in which several different angles are examined close to $\theta = 90^\circ$ and $\theta = 180^\circ$. Within 800 ps, topological charge (sometimes more than 1) quickly switches on and off in the case of $\theta \sim 180^\circ$ due to the constant oscillations driven by the STT. The final state is highly sensitive to the duration of the applied current and the details of the geometry. On the other hand, the topological charge becomes stable in the case of the in-plane polarization. The switching can occur in ~60 ps, after which no further excitations can be initiated and no change of the skyrmion number is witnessed. A similar trend is also observed in the Néel-type skyrmions. This observation is consistent with the skyrmion number oscillation observed in [21]. Small changes in the angle do not strongly affect the switching outcome, indicating that the in-plane polarization is best for creating skyrmions for application purposes.

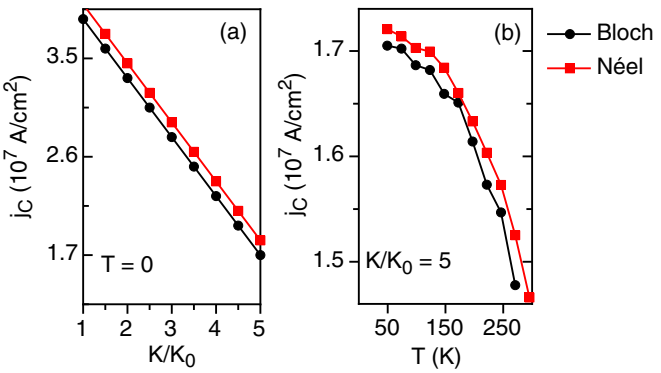

FIG. 6. (a) The reduction of j_C at different values of K. (b) The heat assisted skyrmion creation at finite temperatures. Each point is an average over 400 different sampling runs.

C. Easy-plane anisotropy and heating effects

Although the current density of 10^8 A/cm^2 is still difficult to achieve in applications, the threshold current can be further reduced by an order of magnitude due to easy-plane anisotropy and heating effects. The easy-plane uniaxial anisotropy is written in the Hamiltonian as $H_{\text{ansi}} = \sum_i K V (S_z^i)^2$, where K is the anisotropy energy density and V is the volume of each local spin. This term is physically induced by a combination of the strained structrual effects at the interface and the demagnetization effects due to the aspect ratio. In a helimagnet, it has been proposed that K is measured by K_0, the effective stiffness of the conical phase determined by material parameters (for FeGe, $K_0 = 1.7 \times 10^3$ J/m^3) [32]. Recent experimental results indicate that the skyrmion phase in a FeGe thin film can be significantly extended in the phase diagram, and the value of K/K_0 reaches ~1 when the thickness reduces to 5 nm [33]. Larger values of anisotropy are expected if the thickness further decreases. Since the anisotropy energetically prefers the in-plane configuration, it helps the spin transfer torque to drive the spins to reach the coplanar switching configuration. The required current density can thus be reduced. Starting from the optimum situation in the phase diagram ($\theta = 110^\circ$, $R = 25.3$ nm), the value of K/K_0 is modifed from 1 to 5 in our calculation. As shown in Fig. 6(a), the easy-plane anisotropy reduces the switching current density from by approximately a factor of 2.2 for both types of skyrmions.

The thermal fluctuation given by a finite temperature is further examined numerically. In order to include this effect, a stochastic field $\mathbf{L}$ is added onto the effective field in Eq. (5) [34]. The dissipation-fluctuation relation $\langle L_\mu(\mathbf{r},t) L_\nu(\mathbf{r}',t') \rangle = \xi \delta_{\mu\nu} \delta_{\mathbf{r}\mathbf{r}'} \delta_{tt'}$ is satisfied, where $\xi = \alpha k_B T/\gamma$, and T is the temperature. The average $\langle\ \rangle$ is taken over the realizations of the fluctuation field. The deterministic Heun scheme is employed to integrate out this stochastic LLG equation. Below T_C (270 K in FeGe), the average switching current density based on 400 sampling runs is obtained for both the Néel-type and the Bloch-type skyrmions. The results are shown in Fig. 6(c). Movies recording this process can be found in Ref. [30]. Although thermal fluctuations randomize the local spins at each time step, the overall dynamical process of the skyrmion creation is similar to that at the zero temperature. This demonstrates the stability of the skyrmion creation scheme below T_C. The average switching current density decreases slightly due to the thermal fluctuations, indicating a negligible heat asisted switching effect. Above T_C, although the switching current can be further reduced, the magnetic order starts to vanish, where random topological charges can be spontaneously excited by thermal fluctuations. This should be avoided in the proposed switching scheme.

IV. TOPOLOGICAL PROTECTION

The difficulty of skyrmion switching originates from the critical spin configuration required by the topological

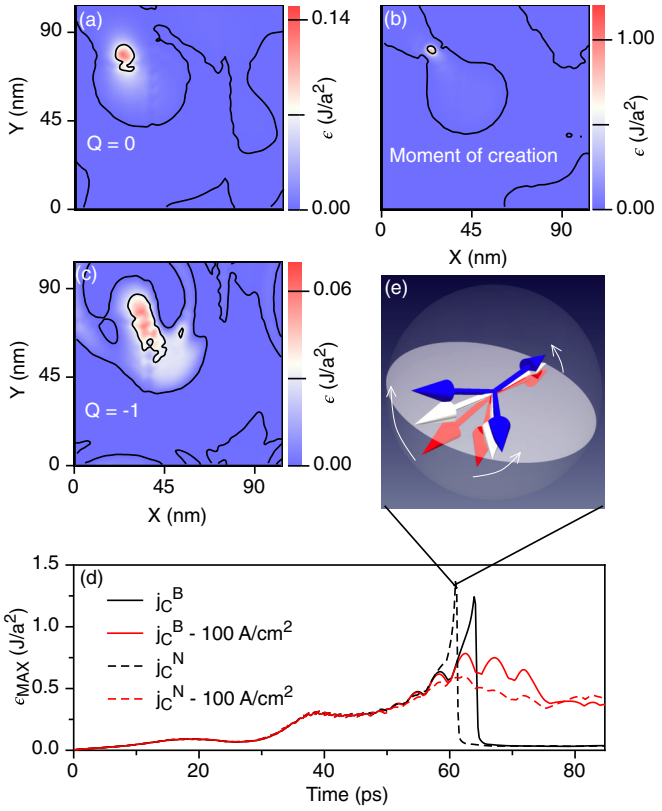

FIG. 7. The energy landscape of the topological transition. (a)–(c) illustrate the energy density distribution of a Bloch-type skyrmion creation process. These plots correspond to the snap shots given in Figs. 4(b)–4(d). The time evolution of the maximum energy density for both types of skyrmions is plotted in (d). (e) illustrates the critical spin configuration when a Néel-type skyrmion is created.

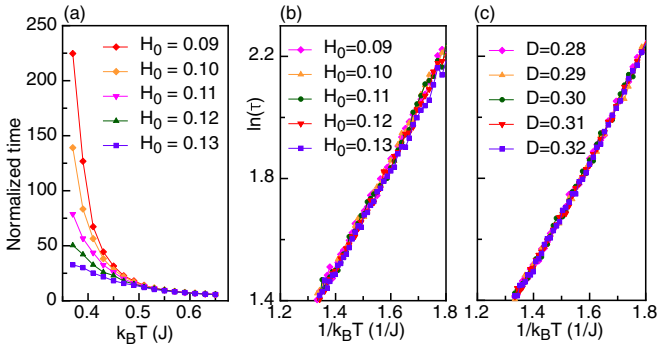

FIG. 8. Average lifetime of a topological charge induced by thermal fluctuations. (a) Single skyrmion life time at finite temperature ($D = 0.3J$, $\alpha = 0.1$). Each point is an average of 1000 sampling runs. (b) and (c), $\ln(\tau)$ vs $1/k_BT$ at different H_0 and D. The slope of the linear fit gives a numerical estimation of $E_a \sim 1.7J$.

transition. The energy landscapes several picoseconds around the moment of creation are shown in Figs. 7(a)–7(c). Exactly at the transition moment, energy is highly concentrated at the switching position, where the energy density overcomes the minimum topological energy barrier, J. For both Néel-type and the Bloch-type skyrmion switching, the maxmium energy density evolves through time, which is plotted in Fig. 7(d). Even when the injected current density is only 100 A/cm^2 below j_C, the energy density cannot overcome the topological barrier, and no skyrmion can be created. Both of the two cases present similar line shapes of the energy evolution, despite the significant differences in the dynamical details (see the movies in Ref. [30]). In both cases, fast skyrmion switching within ~60 ps is achieved. The barrier height of the Néel type is a little larger than that of the Bloch type, which is determined by the exact switching configuration. As shown in Fig. 7(e), the spin alignment is more noncolinear compared to that given in Fig. 4(e), contributing more exchange energy than that of the Bloch type. The difference in this configuration comes from the swirling Oersted field induced by the vertical current. For the Bloch-type skyrmions, the Oersted field helps the in-plane DM interaction form the co-planar texture, while it does not assist the out-of-plane DM interaction in the Néel-type skyrmions. As shown in the phase diagrams in Fig. 5, this difference in the barrier does not significantly affect the switching current density.

This estimate of the topological protection barrier can also be numerically determined from the thermal activation energy. The activation energy of each topological charge is extracted numerically by examining the lifetime of a topological charge as a function of temperature. A skyrmion is simulated at finite temperature until the topological charge switches from -1 to 0 due to the random thermal fluctuations. The time of the annihilation is recorded. This simulation is repeated 1000 times at each temperature, and the average lifetime τ is determined as a function of temperature. Plots of τ versus temperature for different background fields H_0 are shown in Fig. 8(a). At low temperatures, a smaller H_0 results in a more stable single skyrmion with a longer lifetime. At higher temperatures such that k_BT approaches J, all of the curves in Fig. 8(a) converge and decay exponentially. For the transition from skyrmion to ferromagnet, the transition rate k obeys the Arrhenius equation $k \sim \exp(-E_a/k_BT)$. The lifetime τ is the inverse of k so that $\tau \sim 1/k \sim \exp(E_a/k_BT)$. The plot of $\ln\tau$ in Fig. 8(b) is linear in the inverse temperature $1/T$. Plots for various H_0 are nearly parallel with each other with an activation energy of $E_a \sim 1.7J$. Further analysis shows that this activation energy is also insensitive to the DM interaction as shown in Fig. 8(c). The activation energy $E_a \sim 1.7J$ determined from the Arrhenius plots represents the barrier to decay in a skyrmion annihilation process. The maximum activation energy density of 1.25 J per spin determined by direct calculation in Fig. 7(d) represents the energy barrier to creation. These values fall within the range $J < \Delta\epsilon < 2J$ determined from the topological charge analysis leading to Eq. (4), and they support the picture of the topological origin of the activation energy that stabilizes the single skyrmion.

V. CONCLUSIONS

A topological charge analysis provides insight into the locally triggered transition from a trivial to a nontrivial topological spin texture of the Néel or Bloch type skyrmion.

The topological protection of the magnetic skyrmion is determined by the symmetric Heisenberg exchange energy. The topological charge analysis, direct micromagnetic calculation, and extraction from Arrhenius plots created from ensemble averaged finite temperature calculations all give consistent values for the energy barrier determined by the spin geometry at the point of transition between a trivial and nontrivial spin topology of $J < \Delta\epsilon < 2J$. A scheme to create single skyrmions is analyzed for both Néel-type and Bloch-type in helimagnetic thin films utilizing the dynamical excitations induced by the Oersted field and the STT given by a vertically injected spin-polarized current. The critical switching current density is $\sim 10^7$ A/cm^2, which decreases with the easy-plane type uniaxial anisotropy and thermal fluctuations. In-plane spin polarization of the injected current performs better than out-of-plane polarization, and it provides ultrafast switching times (within 100 ps) and reliable switching outcomes.

ACKNOWLEDGMENTS

The micromagnetic simulations, analysis, and writing were supported by the National Science Foundation Grant No. 1408168. The analysis and writing were also supported in part by FAME, one of six centers of STARnet, a Semiconductor Research Corporation program sponsored by MARCO and DARPA. The device design and the experimental discussion were supported in part by the Spins and Heat in Nanoscale Electronic Systems (Spins) an Energy Frontier Research Center funded by the U.S. Department of Energy, Office of Science, Basic Energy Sciences under Award No. DE-SC0012670.

[1] N. Nagaosa and Y. Tokura, Nat. Nanotechnol. **8**, 899 (2013).
[2] U. K. Rößler, A. N. Bogdanov, and C. Pfleiderer, Nature (London) **442**, 797 (2006).
[3] S. Mühlbauer, B. Binz, F. Jonietz, C. Pfleiderer, A. Rosch, A. Neubauer, R. Georgii, and P. Böni, Science **323**, 915 (2009).
[4] X. Z. Yu, Y. Onose, N. Kanazawa, J. H. Park, J. H. Han, Y. Matsui, N. Nagaosa, and Y. Tokura, Nature (London) **465**, 901 (2010).
[5] X. Z. Yu, N. Kanazawa, Y. Onose, K. Kimoto, W. Z. Zhang, S. Ishiwata, Y. Matsui, and Y. Tokura, Nat. Mater. **10**, 106 (2011).
[6] I. Dzyaloshinsky, J. Phys. Chem. Solids **4**, 241 (1958).
[7] T. Moriya, Phys. Rev. **120**, 91 (1960).
[8] N. Kanazawa, Y. Onose, T. Arima, D. Okuyama, K. Ohoyama, S. Wakimoto, K. Kakurai, S. Ishiwata, and Y. Tokura, Phys. Rev. Lett. **106**, 156603 (2011).
[9] J. H. Han, J. Zang, Z. Yang, J.-H. Park, and N. Nagaosa, Phys. Rev. B **82**, 094429 (2010).
[10] W. Munzer, A. Neubauer, T. Adams, S. Muhlbauer, C. Franz, F. Jonietz, R. Georgii, P. Boni, B. Pedersen, M. Schmidt *et al.*, Phys. Rev. B **81**, 041203 (2010).
[11] S. Seki, X. Z. Yu, S. Ishiwata, and Y. Tokura, Science **336**, 198 (2012).
[12] X. Z. Yu, N. Kanazawa, W. Z. Zhang, T. Nagai, T. Hara, K. Kimoto, Y. Matsui, Y. Onose, and Y. Tokura, Nat. Commun. **3**, 988 (2012).
[13] Y. Li, N. Kanazawa, X. Z. Yu, A. Tsukazaki, M. Kawasaki, M. Ichikawa, X. F. Jin, F. Kagawa, and Y. Tokura, Phys. Rev. Lett. **110**, 117202 (2013).
[14] S. Heinze, K. von Bergmann, M. Menzel, J. Brede, A. Kubetzka, R. Wiesendanger, G. Bihlmayer, and S. Blügel, Nat. Phys. **7**, 713 (2011).
[15] F. Jonietz, S. Mühlbauer, C. Pfleiderer, A. Neubauer, W. Münzer, A. Bauer, T. Adams, R. Georgii, P. Böni, R. A. Duine *et al.*, Science **330**, 1648 (2010).
[16] T. Schulz, R. Ritz, A. Bauer, M. Halder, M. Wagner, C. Franz, C. Pfleiderer, K. Everschor, M. Garst, and A. Rosch, Nat. Phys. **8**, 301 (2012).
[17] J. Zang, M. Mostovoy, J. H. Han, and N. Nagaosa, Phys. Rev. Lett. **107**, 136804 (2011).
[18] A. Fert, V. Cros, and J. Sampaio, Nat. Nanotechnol. **8**, 152 (2013).
[19] J. Sampaio, V. Cros, S. Rohart, A. Thiaville, and A. Fert, Nat. Nanotechnol. **8**, 839 (2013).
[20] J. Iwasaki, M. Mochizuki, and N. Nagaosa, Nat. Nanotechnol. **8**, 742 (2013).
[21] N. Romming, C. Hanneken, M. Menzel, J. E. Bickel, B. Wolter, K. v. Bergmann, A. Kubetzka, and R. Wiesendanger, Science **341**, 636 (2013).
[22] Y. Tchoe and J. H. Han, Phys. Rev. B **85**, 174416 (2012).
[23] M. Finazzi, M. Savoini, A. R. Khorsand, A. Tsukamoto, A. Itoh, L. Duò, A. Kirilyuk, T. Rasing, and M. Ezawa, Phys. Rev. Lett. **110**, 177205 (2013).
[24] T. H. R. Skyrme, Proc. R. Soc. London A **260**, 127 (1961).
[25] R. Rajaraman, *Solitons and Instantons* (North-Holland, Amsterdam, 1987).
[26] M. A. Armstrong, *Basic Topology*, 1st ed. (Springer, New York, 1997).
[27] B. Berg and M. Lüscher, Nucl. Phys. B **190**, 412 (1981).
[28] J. Slonczewski, J. Magn. Magn. Mater. **159**, L1 (1996).
[29] B. Behin-Aein, D. Datta, S. Salahuddin, and S. Datta, Nat. Nanotechnol. **5**, 266 (2010).
[30] See Supplemental Material at http://link.aps.org/supplemental/10.1103/PhysRevB.93.174403 for movies on single skyrmion creations for both Bloch and Néel skyrmions at different temperature.
[31] A. Brataas, A. D. Kent, and H. Ohno, Nat. Mater. **11**, 372 (2012).
[32] E. A. Karhu, U. K. Rößler, A. N. Bogdanov, S. Kahwaji, B. J. Kirby, H. Fritzsche, M. D. Robertson, C. F. Majkrzak, and T. L. Monchesky, Phys. Rev. B **85**, 094429 (2012).
[33] S. X. Huang and C. L. Chien, Phys. Rev. Lett. **108**, 267201 (2012).
[34] J. L. García-Palacios and F. J. Lázaro, Phys. Rev. B **58**, 14937 (1998).